Evolution of Narrow-Band Spectra in Deep-Water Constant Vorticity Flows

Christopher W. Curtis and Mackensie Murphy

Introduction

There is now a relatively wide range of literature which shows that nonlinear instabilities, in particular the modulational instability (MI), are responsible for significant modifications to the statistical properties of water waves; see [1, 2, 3, 4] among others. These results have significant impact on the understanding of deep-water rogue wave formation among other oceanographic phenomena. However, much of our understanding around MI relies on highly idealized assumptions which cannot be expected to hold in natural settings. In particular, most understandings of MI rely on looking at the stability of perturbations to carrier waves at essentially a fixed wave number. To address this shortcoming, in a now seminal paper, [5] analytically studies families of perturbations of wave packets with narrow, but non-zero, spectral width around a central wave number. An analytic critierion determining when modulational instability (MI) is either manifested or supressed depending on this spectral width is derived. The results in [5] were confirmed numerically in [1, 2] by examing the mean properties associated with ensembles of initial conditions.

However, many physical effects were ignored in the derivation and verification of the results described above. In particular, vorticity was not taken into account, thereby ignoring a central mechanism for the transfer of energy across length scales in oceanic flows. Thus, building on the work in [4] and [6], we numerically explore the analytic stability condition derived in [5], focusing in particular on the impact that vorticity plays in controlling the effective width for the onset of MI. Moving beyond just examining the properties of the NLS equation with vorticity, we look at the statistical properties of solutions to a higher-order model, the vor-Dysthe equation derived in [6]. As shown in [3], the higher-order terms associated with the Dysthe equation can have significant impacts on the statistics of the waves, so it is a nontrivial question to examine how the vorticity will interact with these higher-order nonlinearities.

Modeling and Stability Theory

We examine the unsteady nonlinear wave propagation over a constant shear current. To do this, we assume the fluid velocity has the form

$$\mathbf{u} = u(\mathbf{x},t)\hat{\mathbf{x}} + w(\mathbf{x},t)\hat{\mathbf{z}} = \omega z\hat{\mathbf{x}} + \nabla\phi,$$

where ϕ is a harmonic function. We restrict fluid motion to the (x,z)-plane, thereby ignoring transverse variations in the y dimension. Following standard arguments, e.g. see [7], the dynamics of the fluid can be determined by solving the free boundary value problem

$$\begin{aligned}
\Delta\phi = 0, \quad & -\infty < z < \eta(x,t), \\
\eta_t + (\omega\eta + \phi_x)\,\eta_x - \phi_z = 0, \quad & z = \eta(x,t), \quad (1)\\
\phi_t + \omega\partial_x^{-1}\eta_t + \frac{1}{2}\left|\mathbf{u}\right|^2 + g\eta - \frac{\sigma}{\rho}\partial_x\frac{\eta_x}{\sqrt{1+\eta_x^2}} = 0, \quad & z = \eta(x,t), \quad (2)\\
\lim_{z\to-\infty}\phi_z = 0, &
\end{aligned}$$

where η represents the free surface displacement, and g, ρ, and σ represent the acceleration due to gravity, the fluid density, and the coefficient of surface tension respectively.

By choosing a characteristic wave height a and wave length L, all quantities can be non-dimensionalized via

$$\begin{aligned}
\tilde{x} = \frac{x}{L},\ \tilde{z} = \frac{z}{L},\ \tilde{t} = \sqrt{\frac{g}{L}}\,t,\ \omega = \sqrt{\frac{g}{L}}\,\tilde{\omega}, \\
\eta = a\tilde{\eta},\ \phi = a\sqrt{gL}\,\tilde{\phi},\ \epsilon = \frac{a}{L}.
\end{aligned}$$

By following the AFM approach described in [8, 7] and dropping the tildes, the kinematic boundary condition, Equation (1), can be written in terms of surface variables alone via the integro-differential equation

$$\int_{\mathbb{R}} dx\ e^{-ikx}e^{\epsilon|k|\eta}\left(\eta_t + \epsilon\omega\eta\eta_x + i\mathrm{sgn}(k)Q\right) = 0,\ k \neq 0, \tag{3}$$

where $Q = q_x$, $q(x,t) = \phi(x,\eta(x,t),t)$. By integrating over $\mathbb{R}$, we are assuming that both η and Q decay to zero sufficiently rapidly in the far field. We can also readily derive a nearly identical expression on domains periodic in the horizontal variable x, in which case Equation (3) becomes

$$\int_{-L_p/2}^{L_p/2} dx\ e^{-ikx}e^{\epsilon|k|\eta}\left(\eta_t + \epsilon\omega\eta\eta_x + i\mathrm{sgn}(k)Q\right) = 0,\ k = \frac{2\pi m}{L_p},\ m \in \mathbb{Z}\backslash 0, \tag{4}$$

where L_p is the spatial period. Throughout the remainder of this section we only present results over the real line, $\mathbb{R}$, since identical results can be

derived for the periodic case. Lastly, we note that if in Equation (3) we approach $k = 0$ from both the left and the right, we get the equations

$$\int_{\mathbb{R}} dx\,(\eta_t + iQ) = 0, \quad \int_{\mathbb{R}} dx\,(\eta_t - iQ) = 0.$$

Thus we get the identities

$$\partial_t \int_{\mathbb{R}} dx\ \eta(x,t) = 0, \tag{5}$$

$$\int_{\mathbb{R}} dx\ Q(x,t) = 0. \tag{6}$$

Taylor expanding Equation (3) up to $\mathcal{O}(\epsilon^3)$ for $k \neq 0$ gives

$$\int_{\mathbb{R}} dx\ e^{-ikx}\left(1 + \epsilon|k|\eta + \frac{\epsilon^2|k|^2\eta^2}{2}\right)(\eta_t + i\mathrm{sgn}(k)Q) + \epsilon\omega\int_{\mathbb{R}} dx\ e^{-ikx}\,(1+\epsilon|k|\eta)\,\eta\eta_x = 0. \tag{7}$$

Transforming into surface variables and Taylor expanding Equation (2), Bernoulli's equation, up to $\mathcal{O}(\epsilon^3)$ gives

$$Q_t + \omega\eta_t + \eta_x - \tilde{\sigma}\eta_{xxx} + \frac{\epsilon}{2}\partial_x\left(-\eta_t^2 + (Q+\omega\eta)^2\right) + \epsilon^2\partial_x\left(\frac{3}{2}\tilde{\sigma}\eta_x^2\eta_{xx} - \eta_t\eta_x\,(Q+\omega\eta)\right) = 0, \tag{8}$$

where the reciprocal of the Bond number, $\tilde{\sigma}$, is given by

$$\tilde{\sigma} = \frac{\sigma}{\rho g L^2}.$$

We note that we have tacitly assumed $\omega = \mathcal{O}(1)$. In physical terms, this implies that ω is comparable to the natural time scale of this problem, $\sqrt{L/g}$. If we were to assume ω were of larger magnitude, the problem would no longer be weakly nonlinear and would be much less amenable to asymptotic analysis. Therefore, throughout the remainder of the paper, we assume that the vorticity is not too large.

In non-dimensional variables, we model the evolution of a relatively small free-fluid surface over infinitely-deep water $z = \epsilon\eta(x,t)$ via the expansion

$$\eta(x,t) = \eta_1(\xi,\tau)e^{i\theta(x,t)} + \eta_1^*(\xi,\tau)e^{-i\theta(x,t)} + \epsilon\left(\eta_0(\xi,\tau) + \eta_2(\xi,\tau)e^{2i\theta(x,t)} + \eta_2^*(\xi,\tau)e^{-2i\theta(x,t)}\right) + \mathcal{O}\left(\epsilon^2\right)$$

where $\tau = \epsilon^2 t$, $\xi = \epsilon(x + c_g t)$, and $\theta(x,t) = k_0 x + \Omega(k_0,\omega)t$, where the linear dispersion relationship $\Omega(k_0,\omega)$ is given by

$$\Omega(k_0,\omega) = \frac{1}{2}\left(s\omega \pm \sqrt{\omega^2 + 4|k_0|\left(1+\tilde{\sigma}k_0^2\right)}\right).$$

Here, $s = \mathrm{sgn}(k_0)$, ω is the non-dimensionalized magnitude of the vorticity of the flow, and $\tilde{\sigma}$ is the surface tension.

To describe the evolution of the slowly evolving envelope $\eta_1(\xi, \tau)$, we use two asymptotically accurate models. The first model is the the nonlinear Schrödinger equation (NLSE) derived in [6], though see also [4], given by

$$i\partial_\tau \eta_1 + \alpha_d \partial_\xi^2 \eta_1 + \alpha_{nl} |\eta_1|^2 \eta_1 = 0,$$

where

$$\begin{aligned} c_g =& \frac{1 + 3\tilde{\sigma} k_0^2}{2s\Omega - \omega}, \\ \alpha_d(k_0, \omega) =& \frac{(c_g^2 - 3|k_0|\tilde{\sigma})}{2\Omega - s\omega}, \\ \alpha_{nl}(k_0, \omega) =& \frac{k_0 \left(s k_0^3 \left(8 + \tilde{\sigma} k_0^2 + 2(\tilde{\sigma} k_0^2)^2 \right) + \omega \alpha_v \right)}{(2s\Omega - \omega)(1 + c_g \omega) \left(4\Omega^2 - s(2k_0(1 + 4\tilde{\sigma} k_0^2) + 2\omega\Omega) \right)}. \end{aligned}$$

The second model we study in this paper is a higher-order generalization of the NLSE which we call the vor-Dysthe Equation (VDE) which was derived in [6]. In this paper, we use it in the form

$$i\partial_\tau \eta_1 + \alpha_d \partial_\xi^2 \eta_1 + \alpha_{nl} |\eta_1|^2 \eta_1 - \epsilon \frac{i(2sc_g \alpha_d + \tilde{\sigma})}{\omega - 2s\Omega} \partial_\xi^3 \eta_1 + i\epsilon \mathcal{N}(\eta_1) = 0,$$

where

$$\mathcal{N}(\eta_1) = \tilde{\alpha}_1 |\eta_1|^2 \partial_\xi \eta_1 + \tilde{\alpha}_2 \eta_1^2 \partial_\xi \eta_1^* + i\tilde{\alpha}_3 \eta_1 \mathcal{H} \partial_\xi |\eta_1|^2 + \tilde{\alpha}_4 \partial_\xi |\eta_1|^2 \eta_1,$$

and $\mathcal{H}$ is the Hilbert transform. The terms $\tilde{\alpha}_j$ are straightforward to derive with the aid of a program like SAGE, but they are lengthy and not illuminative, and thus they are ommitted for the sake of brevity.

To generate simulations, we start both the NLSE and VDE from the same collection of $2L$ periodic-initial conditions

$$\eta_1(\xi, 0) = \epsilon_{rms} \sqrt{\frac{\delta\tilde{k}}{\sigma\sqrt{\pi}}} \sum_{k=-K+1}^{K} e^{-\tilde{k}^2/2\sigma^2} e^{i\theta_k} e^{i\tilde{k}\xi}, \ \tilde{k} = \frac{\pi k}{L},$$

where $\delta\tilde{k} = \pi/L$ and the phases θ_k are randomly chosen uniformly between 0 and 2π. We can then readily show that, for $L \gg 1$,

$$\epsilon_{rms} \approx \overline{|\eta_1|^2}^{1/2},$$

where $\overline{()}$ denotes the ensemble average. In our coordinates then, the work in [5] and later confirmed in [1] shows that for the NLSE the MI is suppressed for spectral widths σ such that

$$\sigma \geq \epsilon_{rms} \sqrt{\frac{2\alpha_{nl}}{\alpha_d}}$$

This work has helped motivate defining this parameter as the Benjamin–Feir Index (BFI), which has been shown to be a critical parameter to understanding the statstical properties of nonlinear free-surface flows; see [3, 4].

Results

To understand the relationship between the vorticity ω and the initial spectral width σ of our initial conditions, we generate ensembles of initial conditions and then run these different initial conditions up to $\tau = 1$, which corresponds to $t_f = 1/\epsilon^2$ in the original fast variables. The domain is $[-50\pi, 50\pi]$. The number of modes is $K = 256$. The surface tension is $\tilde{\sigma} = 10^{-5}$. We then plot the averaged spectral density $S(k, t_f; \sigma)$ where

$$S\left(k, t_f; \sigma\right) = \overline{\left(\left|\frac{1}{\epsilon}\hat{\eta}_1\left(\frac{k-k_0}{\epsilon}, 1; \sigma\right)\right|^2\right)}.$$

which corresponds to the autocorrelation of the surface profile with respect to space. Note we have emphasized the dependence on the initial spectral width σ for the sake of clarity. Following the approach in [1, 2], by comparing the initial spectral density to that at later times, we can see directly whether MI manifests as significant distortions of the statistics, or if through supression the distributions remain relatively close to one another.

Throughout our results, we have used a psuedo-spectral method in space coupled with a 4th-order Runge-Kutta scheme using integrating factors in time, with a time step of $dt = 2.5 \times 10^{-3}$. De-aliasing is implemented via Orszag's '2/3-rule'. Averaging was done with $N_e = 3200$ ensemble members, thereby ensuring relative averaging errors on the order of about 1%. Throughout this section, we present comparisons of the distributions for particular choices of σ while also comparing the mean and standard deviations of the respective distributions so as to get a more quantitative understanding of the differences between the different distributions.

Strong-Counter Shear: $\omega = -1$

Motivated by the results in [6], we anticipate that $\omega = -1$ presents the most case which would allow for the vorticity to have the strongest impact on the BFI condition, which for the parameter choices requires that $\sigma > 11.9$. This is borne out by numerical experiment as seen in Figures 1 and 2. In this case, we see that for the NLSE the BFI condition largely holds. In particular, we see that while the mean never changes in any significant way from that of the initial distribution, increasing the width σ causes the standard deviation of the distribution determined via evolution of the NLSE to collapse onto that of the initial, thereby showing that wider spreads in initial conditions are overall less susceptible to MI.

However, the results for the VDE are markedly different. As seen in Figure 2, where $\sigma = 12$ so that we are just past the BFI threshold, the most peculiar feature of the VDE is the bimodality of the distribution. There is clearly a frequency downshift of the central initial peak, but a secondary

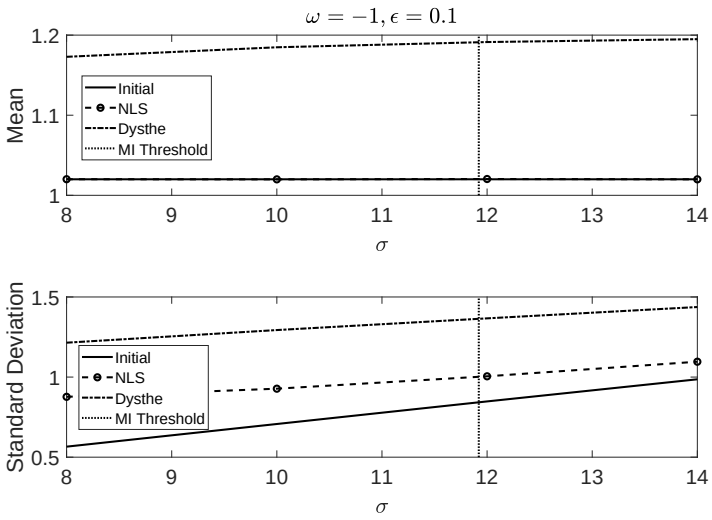

(a) $\epsilon = .1$

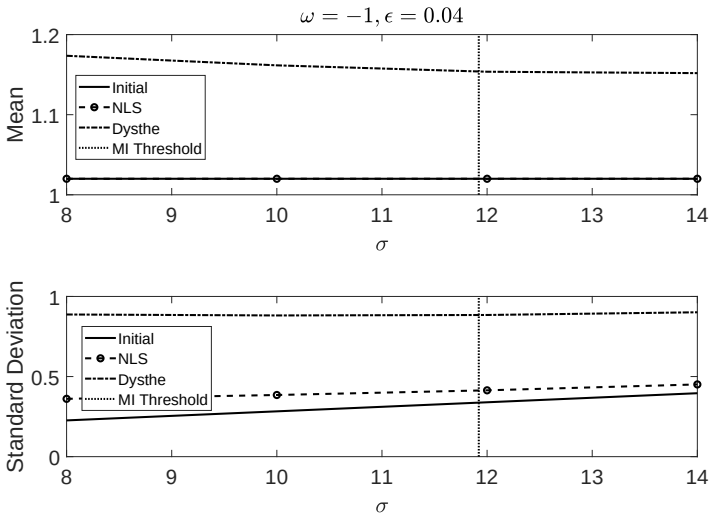

(b) $\epsilon = .04$

Figure 1: For $\omega = -1$, comparison of the means and standard deviations between the initial averaged spectral density and those generated by the NLSE and VDE. This is shown for varying strengths of the small amplitude, and thus nonlinearity, parameter ϵ with $\epsilon = .1$ in (a) and $\epsilon = .04$ in (b). The vertical line denotes the spectral width corresponding to the BFI condition.

peak at high-wave number forms as well. This formation is less pronounced with decreasing ϵ, but is clearly there nevertheless. This represents a kind of resonance condition for which no ready explanation exists. This feature

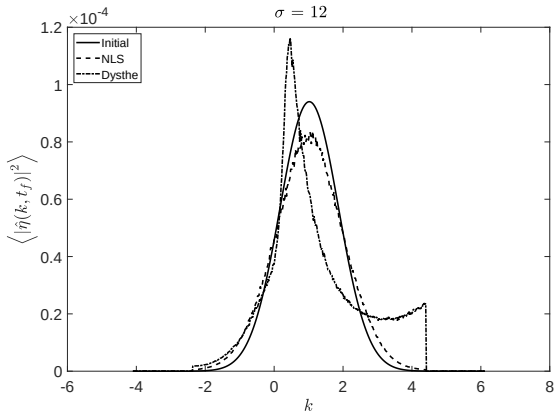

(a) $\epsilon = .1$

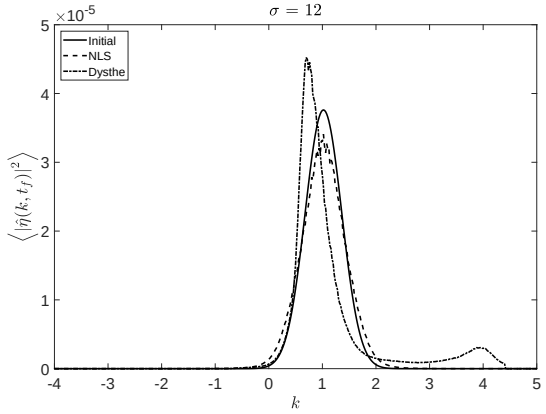

(b) $\epsilon = .04$

Figure 2: For $\omega = -1$, comparison of the averaged spectral densities between the initial averaged spectral density and those generated by the NLSE and VDE. This is shown for varying strengths of the small amplitude, and thus nonlinearity, parameter ϵ with $\epsilon = .1$ in (a) and $\epsilon = .04$ in (b).

is likewise responsible for the strong skewing of the means and standard deviations seen in Figure 1.

Vorticity-Free Flow: $\omega = 0$

Removing vorticity, we see that we essentially recreate the standard BFI, with BFI threshold $\sigma > 5.7$, results for the NLSE. Again though, the VDE produces markedly different statistical results from the NLS, though to nowhere near as drastic an extent as when $\omega = -1$. In particular, the bimodality and strong deformation of the profile is notably ameliorated for $\epsilon = .04$; see Figures 3 and 4. Thus in some sense, though not entirely, MI has more or less similar characteristics for both the NLSE and VDE.

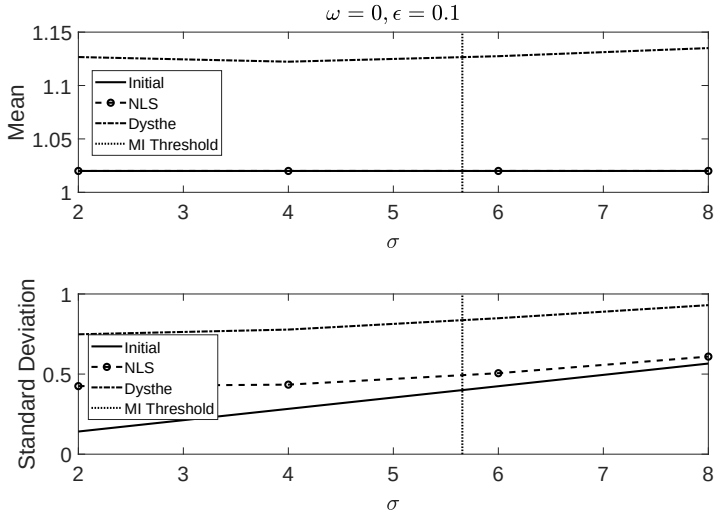

(a) $\epsilon = .1$

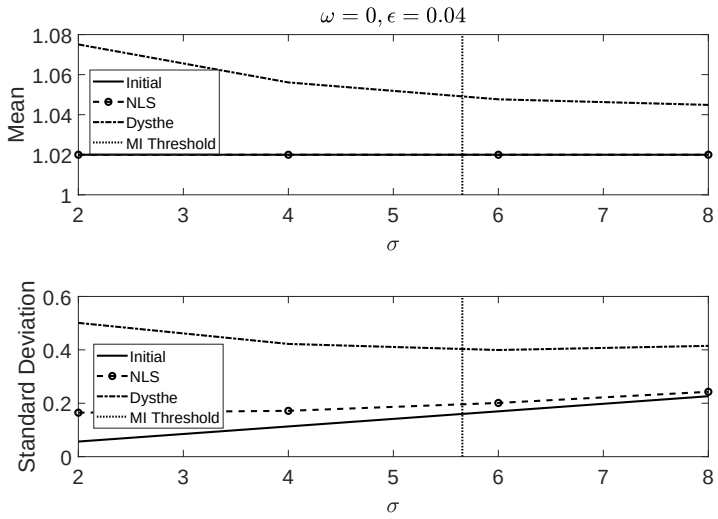

(b) $\epsilon = .04$

Figure 3: For $\omega = 0$, comparison of the means and standard deviations between the initial averaged spectral density and those generated by the NLSE and VDE. This is shown for varying strengths of the small amplitude, and thus nonlinearity, parameter ϵ with $\epsilon = .1$ in (a) and $\epsilon = .04$ in (b). The vertical line denotes the spectral width corresponding to the BFI condition.

Strong-Co Shear: $\omega = 1$

Finally, by letting $\omega = 1$, we further reduce the BFI threshold to $\sigma > 2.7$, opening up a yet wider range of stable initial conditions. Likewise, the VDE

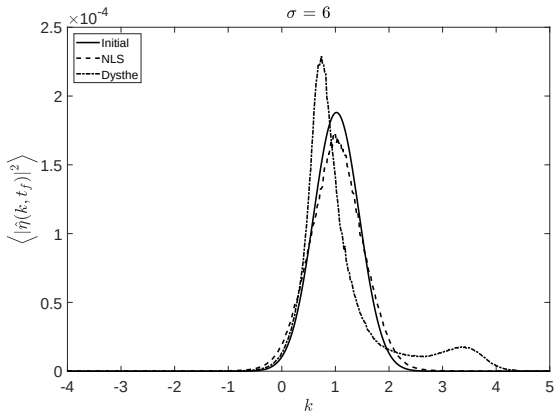

(a) $\epsilon = .1$

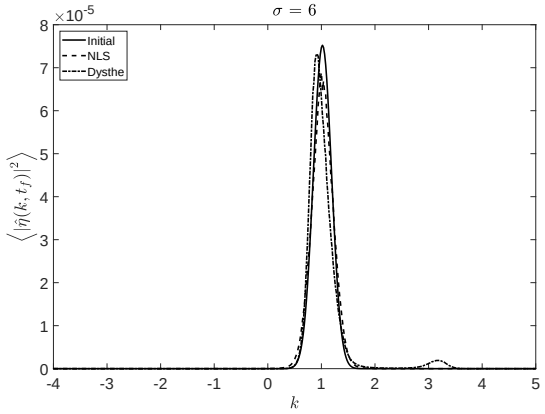

(b) $\epsilon = .04$

Figure 4: For $\omega = 0$, comparison of the averaged spectral densities between the initial averaged spectral density and those generated by the NLSE and VDE. This is shown for varying strengths of the small amplitude, and thus nonlinearity, parameter ϵ with $\epsilon = .1$ in (a) and $\epsilon = .04$ in (b).

dynamics are far more in line with those seen from the NLSE, even in the case that $\epsilon = .1$; see Figures 5 and 6. Therefore, we see how vorticity propagating in the correct direction can vastly reduce the impact of MI, even in a far more nonlinear model like the VDE.

Conclusion

References

[1] K.B. Dysthe, K. Trulsen, H.E. Krogstad, and H. Socquet-Juglard. Evolution of a narrow-band spectrum of random surface gravity waves. *J.*

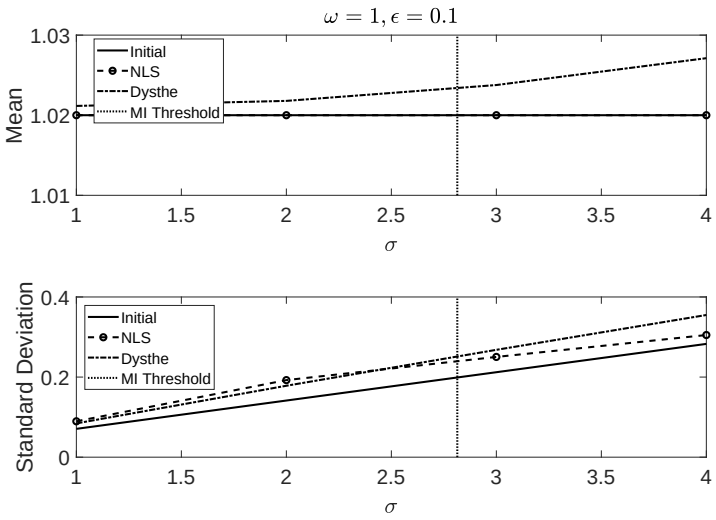

(a) $\epsilon = .1$

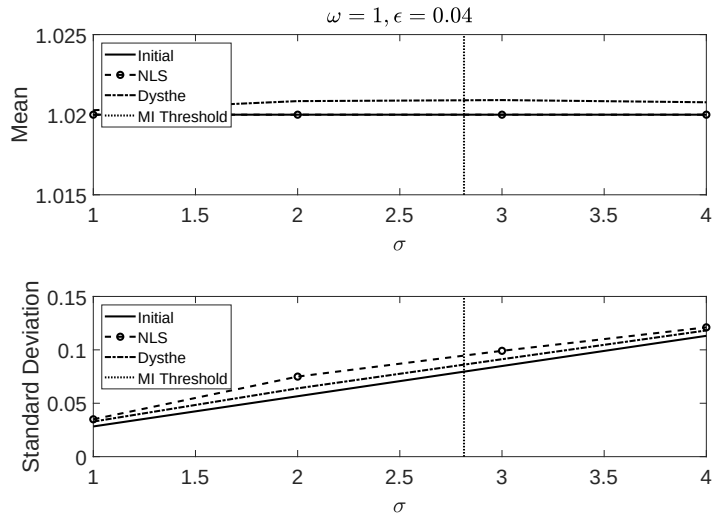

(b) $\epsilon = .04$

Figure 5: For $\omega = 1$, comparison of the means and standard deviations between the initial averaged spectral density and those generated by the NLSE and VDE. This is shown for varying strengths of the small amplitude, and thus nonlinearity, parameter ϵ with $\epsilon = .1$ in (a) and $\epsilon = .04$ in (b). The vertical line denotes the spectral width corresponding to the BFI condition.

Fluid Mech., 478:1–10, 2003.

[2] H. Socquet-Juglard, K.B. Dysthe, K. Trulsen, and H.E. Krogstad. Probablity distributions of surface gravity waves during spectral changes. *J.*

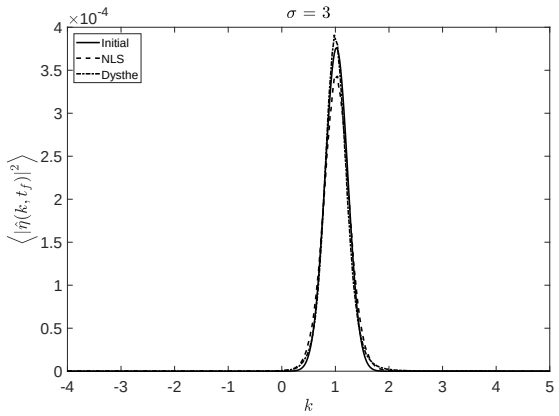

(a) $\epsilon = .1$

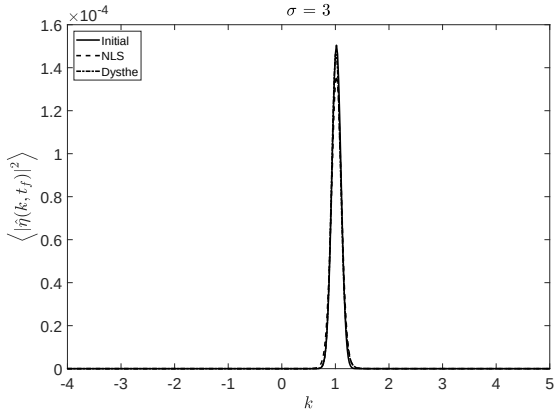

(b) $\epsilon = .04$

Figure 6: For $\omega = 1$, comparison of the averaged spectral densities between the initial averaged spectral density and those generated by the NLSE and VDE. This is shown for varying strengths of the small amplitude, and thus nonlinearity, parameter ϵ with $\epsilon = .1$ in (a) and $\epsilon = .04$ in (b).

Fluid Mech., 510:195–216, 2005.

[3] M. Onorato, A.R. Osborne, M. Serio, L. Cavaleri, C. Brandini, and C.T. Stansberg. Extreme waves, modulational instability and second order theory: wave flume experiments on irregular waves. *Eur. J. Mech. B Fluids*, 22:586–601, 2006.

[4] R. Thomas, C. Kharif, and M. Manna. A nonlinear Schrödinger equation for water waves on finite depth with constant vorticity. *Phys. Fluids*, 24(12):127102, 2012.

[5] I.E. Alber. The effects of randomness on the stability of two-dimensional surface wavetrains. *Proc. Roc. Soc. A*, 363:525–546, 1978.

[6] C.W. Curtis, J.C. Carter, and H. Kalisch. Particle paths in nonlinear Schrödinger models in the presence of linear shear currents. *J. Fluid Mech.*, to appear.

[7] A.C.L. Ashton and A.S. Fokas. A non-local formulation of rotational water waves. *J. Fluid Mech.*, 689:129–148, 2011.

[8] M.J. Ablowitz, A.S. Fokas, and Z.H. Musslimani. On a new non-local formulation of water waves. *J. Fluid Mech.*, 562:313–343, 2006.